



Photocatalytic degradation of Congo red by using the $\text{Cu}_2\text{O}/\alpha\text{-Fe}_2\text{O}_3$ composite catalyst

Zhuohao Li^a, Xiuting Chen^a, Miao Wang^a, Xia Zhang^a, Lixia Liao^{a,b}, Tao Fang^{a,b,*}, Bin Li^{a,*}

^aCollege of Chemistry, Chemical Engineering and Resource Utilization, Northeast Forestry University, Harbin 150040, China, emails: nefuft@hotmail.com (T. Fang), libinzh62@163.com (B. Li), 974989897@qq.com (Z.H. Li), 929885427@qq.com (X.T. Chen), 811480182@qq.com (M. Wang), 1870776231@qq.com (X. Zhang), lxiao1024@126.com (L.X. Liao)

^bSchool of Chemical Engineering, Purdue University, West Lafayette, IN 47907, USA

Received 15 April 2020; Accepted 13 November 2020

ABSTRACT

The $\text{Cu}_2\text{O}/\alpha\text{-Fe}_2\text{O}_3$ photocatalytic composites were synthesized by precipitation method. The synthesized $\alpha\text{-Fe}_2\text{O}_3$ and $\text{Cu}_2\text{O}/\alpha\text{-Fe}_2\text{O}_3$ were characterized by scanning electron microscopy, X-ray diffraction and X-ray photoelectron spectroscopy. The effects of the $\alpha\text{-Fe}_2\text{O}_3$ synthesis method, Cu_2O mass ratio, initial concentration of Congo red, catalyst quality, reaction temperature and initial pH on the degradation rate of Congo red were investigated. The results showed that under the irradiation of a high-pressure mercury lamp, 12 mg $\text{Cu}_2\text{O}/\alpha\text{-Fe}_2\text{O}_3$ as a photocatalyst, in which the mass fraction of Cu_2O is 5%, initial pH of 6.0, degradation of 100 mL and 25 mg L⁻¹ Congo red solution for 60 min, the best degradation rate of Congo red can reach 95.57%. Under the optimized conditions, the chemical oxygen demand and total organic carbon removal rates of Congo red reached 85.36% and 72.57%, respectively. The reaction kinetic of Congo red degradation was according to the pseudo-first-order reaction kinetic model, and the possible mechanism of the photocatalytic reaction was also discussed.

Keywords: Photocatalysis; Congo red; Cu_2O ; $\alpha\text{-Fe}_2\text{O}_3$

1. Introduction

Using sunlight for photocatalytic degradation of organic dye wastewater is a green energy-saving treatment method, which has potential application value to solve current energy and environmental problems. In general, wide bandgap semiconductor photocatalysts, such as TiO_2 [1], ZnO [2], etc., photodegradation of organic pollutants under ultraviolet light has been widely used in wastewater treatment, due to their own characteristics. However, the proportion of ultraviolet light in the solar spectrum only 3%–5% [3]. Therefore, the efficiency and commercial viability of the wide-gap photocatalysts are greatly limited. The proportion of visible light almost 43% of the solar spectrum [4], if we can make full use of this part of the

light source, it can bring huge economic and social benefits. Based on this reason, many researchers have focused on semiconductors in the visible region by loading a transition metal or adding a low bandgap semiconductor as a sensitizer [5–11]. The rapid recombination of charge carriers is largely circumvented by designing heterogeneous or homogenous connections between metal oxides to enhance its photocatalytic efficiency. Therefore, compared with a single metal oxide semiconductor, it has higher charge transfer efficiency and photocatalytic activity [12].

For the past few years, iron oxide in the form of mixed metal oxides was widely concerned because of its narrow bandgap (2.1 eV) [13,14]. In addition, due to the Fe^{2+} and Fe^{3+} ion oxidation-reduction reactions, the $\alpha\text{-Fe}_2\text{O}_3$ Fenton

* Corresponding authors.

reaction can produce a large amount of OH^{\bullet} , which greatly promotes the decomposition of toxic substances and organic pollutants in wastewater [15]. However, it is well known that due to the high recombination rate of electrons and holes generated in the photocatalytic reaction, the most stable iron oxide photocatalytic activity in $\alpha\text{-Fe}_2\text{O}_3$ is usually not very stable [16]. So we can improve the separation of charge carriers and increase the photocatalytic activity of $\alpha\text{-Fe}_2\text{O}_3$ by designing of the homogenous junction and the heterogeneous junction between the metal oxides.

Some researchers have improved photocatalytic performance by mixing or doping photocatalyst under visible light. $\alpha\text{-Fe}_2\text{O}_3/\text{g-C}_3\text{N}_4$ Z-scheme photocatalyst was synthesized, which can improve quantum efficiency, and used to catalyze the overall water splitting reaction [17]. The 3D flowerlike $\alpha\text{-Fe}_2\text{O}_3/\text{TiO}_2$ core-shell nanocrystals with rhombohedral, cubic and decal morphologies were prepared for the degradation of Rhodamine B [18]. The researchers discussed its comprehensive performances and durability of its photocatalysis in a heterogeneous Fenton system, where the $\alpha\text{-Fe}_2\text{O}_3$ is anchored to graphene oxide (GO) nanosheet ($\alpha\text{-Fe}_2\text{O}_3/\text{GO}$) through a mild hydrolysis process [19]. The $\alpha\text{-Fe}_2\text{O}_3/\text{Bi}_2\text{MoO}_6$ heterostructure has been synthesized by the electrospinning the combined calcining process, and the photodegradation of Methylene blue under the simulated sunlight have obtained, the higher degradation rate of $\alpha\text{-Fe}_2\text{O}_3/\text{Bi}_2\text{MoO}_6$ heterostructure can be reached than pure Bi_2MoO_6 nanofibers and pure TiO_2 [20].

Cu_2O is a p-type semiconductor with a direct bandgap of 2.2 eV, because of its photocatalytic property in visible light, we can use its characteristics to improve the photocatalytic performance of composite photocatalyst. Unlike the TiO_2 (3.2 eV) photocatalyst, TiO_2 can only utilize ultraviolet and near-ultraviolet light. Therefore, Cu_2O is an economical and practical photocatalyst with great potential application value. In the Cu_2O photocatalytic system, the photogenerated hole potential of Cu_2O is lower than the oxidation potential of H_2O , and H_2O cannot be oxidized to OH^{\bullet} , but Cu_2O has a strong ability to adsorb oxygen molecules, O_2 adsorption can react with water and photogenerated electrons redox to form H_2O_2 and OH^{\bullet} , which has strong oxidizing properties, thus oxidizing organic substances into small molecules such as CO_2 and water [21]. Researchers found that the Cu_2O film with the synergistic effect of H_2O_2 under visible light irradiation for 2 h, the degradation rate of Methyl orange reached almost 100% [22,23]. Nguyen et al. [24] discovered that Cu_2O octahedral microcrystals have a good photocatalytic degradation effect on Methyl orange, but the catalytic degradation of Methylene blue is an extremely bad effect. Ren et al. [25] prepared sandwich-like $\text{ZnO}/\text{Ag}/\text{Cu}_2\text{O}$ and $\text{ZnO}/\text{Au}/\text{Cu}_2\text{O}$ film samples. The experimental results showed that Ag-plasmon resonance can promote the separation of e^- and h^+ , and the Schottky junction formed by Ag and Cu_2O can prevent the recombination of e^- and h^+ , thereby increasing the catalytic degradation rate of Methyl orange. Because cuprous oxide and iron oxide can absorb visible light well, and they have abundant resources, the combination of Cu_2O and $\alpha\text{-Fe}_2\text{O}_3$ to prepare photocatalysts to degrade organic matter has attracted the attention of many researchers. Wang et al. [26] reported that the hematite-cuprous oxide ($\alpha\text{-Fe}_2\text{O}_3/\text{Cu}_2\text{O}$)

nanocomposites were designed based on the Z-scheme photocatalyst used to reduce carbon dioxide. Lakhera et al. [27] prepared an efficient binary $\alpha\text{-Fe}_2\text{O}_3/\text{Cu}_2\text{O}$ mixed metal oxide photocatalysts was used to degrade Methyl orange by hydrothermal method. However, the degradation of Congo red organic pollutants was rarely reported by the $\text{Cu}_2\text{O}/\alpha\text{-Fe}_2\text{O}_3$ mixed metal oxide catalyst.

In this paper, $\text{Cu}_2\text{O}/\alpha\text{-Fe}_2\text{O}_3$ composite catalysts were prepared by a two-step method. Although Cu_2O has a high catalytic degradation rate for organic substances such as Methyl orange, the redox potential for Cu^+ is between the forbidden band of Cu_2O and it is easily reduced to Cu elemental substance in photoelectrochemical reaction to poor stability. The $\alpha\text{-Fe}_2\text{O}_3$ was synthesized by hydrothermal method, then a new photocatalytic compound catalyst was obtained by co-deposition with Cu_2O . The photocatalytic properties of $\text{Cu}_2\text{O}/\alpha\text{-Fe}_2\text{O}_3$ composites were tested for water-soluble organic Congo red as simulation research material, the molecular structure of Congo red is shown in Fig. 1. Several factors affecting the efficiency of photocatalytic degradation of Congo red by composite photocatalytic materials were studied.

2. Experiments section

2.1. Synthesis of $\alpha\text{-Fe}_2\text{O}_3$

Method 1: Accurately weight 0.002 mol $\text{FeCl}_3 \cdot 6\text{H}_2\text{O}$ and 0.1802 g urea and 0.00216 mol sodium dodecylbenzenesulfonate into the 30 mL beaker, and then measure 30 mL of *n*-butanol into the beaker to form a mixture solution. Stir at room temperature for 15 min to dissolve all solids in the solution. The solution was poured into a 100 mL polytetrafluoroethylene autoclave and placed in an electric blast drying oven at a set temperature of 150°C for 15 h. When the oven is completely cool to room temperature, the reaction vessel is taken out to obtain a red solid precipitate, which is washed three times with an appropriate amount of deionized water and absolute ethanol and centrifuged to separate the product, and the product obtained after washing is placed in a vacuum drying oven. Set the reaction temperature of 60°C, dry under vacuum for 12 h to obtain a red solid, and grind the sample to obtain the final product (C1).

Method 2: Accurately weight 0.003 mol $\text{FeCl}_3 \cdot 6\text{H}_2\text{O}$ and 1.0 g PVP into an 80 mL ethanol solution consisting of 40 mL absolute ethanol and 40 mL deionized water, and vigorously stir at room temperature for 3 h. The solids in the solution are all dissolved and mixed. The solution was poured into a 100 mL polytetrafluoroethylene autoclave at 170°C for 3 h. After the oven is naturally cool to room temperature, the solution is centrifuged to obtain a solid, which is washed three times with deionized water and absolute ethanol, respectively. The obtained product is placed in a 60°C vacuum oven and dried for 10 h, the obtained sample is ground to obtain the final product (C2).

Method 3: Dissolve 346 mg of ferric chloride hexahydrate in a beaker containing 150 mL of deionized water for 15 min, then add 10 mg of sodium dihydrogen phosphate particles, and finally transfer the solution to 200 mL high-pressure reactor, at last, put into a blast drying oven, set the temperature of 200°C, hydrothermal reaction for 8h,

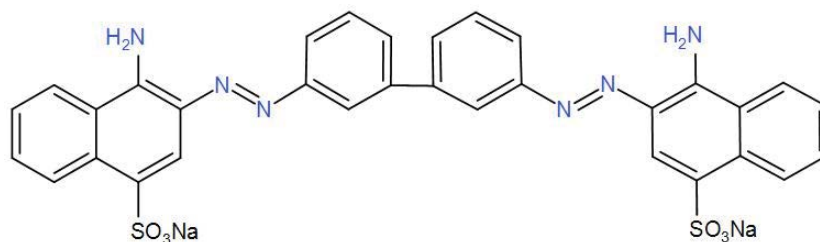


Fig. 1. Molecular structure of Congo red.

and then experiment end, pour out the solution. Finally, the sample was placed in a 50°C vacuum drying oven, and the drying time was 18 h to obtain nano- α -Fe₂O₃ (C3).

2.2. Synthesis of Cu₂O/ α -Fe₂O₃

Add 0.05 g of CuSO₄·5H₂O to 100 mL 0.1 mol L⁻¹ cetyltrimethylammonium bromide solution and fully dissolve, then ultrasonically disperse the above α -Fe₂O₃ in the solution, add 0.18 g ascorbic acid to the mixed solution and heat of 60°C to keep 20 min. A yellow precipitate was added to 10 mL 0.2 mol L⁻¹ sodium hydroxide solution, stirred for 10 min, centrifuged, rinsed several times with deionized water and ethanol, and then vacuum dried at 50°C for 5 h [28].

2.3. Characterization

In this experiment, the product was characterized by X-ray diffractometry and scanning electron microscopy (SEM). The X-ray (TD-3500) diffractometer adopts the scanning parameters as the starting angle: 10°, the ending angle: 80°, the step width angle: 0.04, and the sampling time: 0.5 s t⁻¹. Before the scanning electron microscope operation (EM30; ETD-2000), the product was dispersed with absolute ethanol and sonicated for 20 min, placed on the sample stage, and sputtered with a small ion sputtering apparatus. The gold target was selected, and the sputtering current was 10 mA at the working voltage. Spray gold for 2 min at 220 V. Then, a scanning electron microscope operation is performed to obtain an electron microscope image of the product. X-ray photoelectron spectroscopy (XPS) was recorded on PHI 5700 ESCA system.

2.4. Photocatalytic activity

Accurately weight 30 mg Congo red with analytical balance, dissolve in 100 mL beaker, transfer to 1,000 mL volumetric flask, add distilled water to make Congo red solution concentration of 30 mg L⁻¹. The schematic diagram of the photocatalysis experiment device is shown in Fig. 2. The maximum absorption wavelength of Congo red is 497 nm measured by an ultraviolet-visible spectrophotometer. In this experiment, the photocatalytic degradation rate was explored by using a single variable, the influence of degradation Congo red solution such as different catalyst synthesis methods, composite material ratio, composite photocatalyst dosage, degradation temperature, reaction pH, and initial concentration of Congo red was investigated.

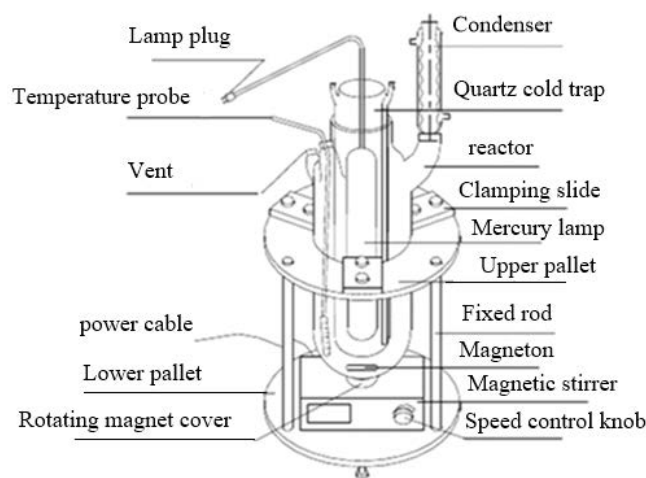


Fig. 2. Structure diagram of photocatalysis experiment device.

Evaluation of the Cu₂O/ α -Fe₂O₃ photocatalytic performance by the degradation rate of Congo red. Calculate the degradation rate of Congo red according to the following formula:

$$\eta = \frac{(C_0 - C_t)}{C_0} \times 100\% = \frac{(A_0 - A_t)}{A_0} \times 100\% \quad (1)$$

where η is the photocatalytic degradation rate, C_0 is the initial Congo red concentration, C_t is the Congo red concentration after the reaction. A_0 is the absorbance of the wastewater solution before the reaction, A_t is the absorbance of the wastewater solution after the reaction time.

2.5. Catalyst characterization

2.5.1. Phase structure X-ray diffraction

Fig. 3a shows the X-ray diffraction patterns of α -Fe₂O₃ with different preparation methods. There are characteristic diffraction peaks at $2\theta = 24.1^\circ, 33.1^\circ, 35.6^\circ, 40.9^\circ, 49.5^\circ, 54.1^\circ, 62.4^\circ$ and 64.0° that correspond to (012), (104), (110), (113), (024), (116), (214) and (300) lattice planes in bare α -Fe₂O₃. Fig. 3a shows that the products prepared by the three synthetic methods are all α -Fe₂O₃ comparing with the α -Fe₂O₃ standard card. And the diffraction peaks of bare Cu₂O are observed at $2\theta = 29.9^\circ, 37.0^\circ, 42.6^\circ, 62.4^\circ$ and 74.4° . Because the load is too small, there is no sign Cu₂O of significant growth in Figs. 3b3, b4 and b5. However, the Cu₂O/ α -Fe₂O₃

composite catalyst with a doping amount of 20% shows the diffraction peaks at 37.0° and 42.6° that correspond to (111) and (200) lattice planes, respectively.

From Fig. 3b it can be clearly seen that with the increase of Cu_2O doping amount, the characteristic peak diffraction intensity of $\alpha\text{-Fe}_2\text{O}_3$ itself decreases. It is very likely that the surface growth of Cu_2O particles affects the crystallinity of $\alpha\text{-Fe}_2\text{O}_3$ and its photocatalytic activity.

2.5.2. Surface morphology scanning electron microscopy

From Fig. 4 SEM images, we can see that the prepared C1 is a quasi-cube (Fig. 4a), the C2 is cubic and spherical

particles (Fig. 4b), and the C3 is composed of spherical and irregular particles (Fig. 4c). Fig. 4d is the SEM of the $\text{Cu}_2\text{O}/\alpha\text{-Fe}_2\text{O}_3$ composite photocatalyst. The prepared composite photocatalyst has fine particles on the spherical particles of $\alpha\text{-Fe}_2\text{O}_3$, which are composite Cu_2O particles. There are black potholes on the surface of the particles, that is, the existing surface defect.

2.5.3. Material structure valence X-ray photoelectron spectroscopy

Fig. 5a shows the XPS spectra of 5% $\text{Cu}_2\text{O}/\alpha\text{-Fe}_2\text{O}_3$. The corresponding peak position is calibrated according to

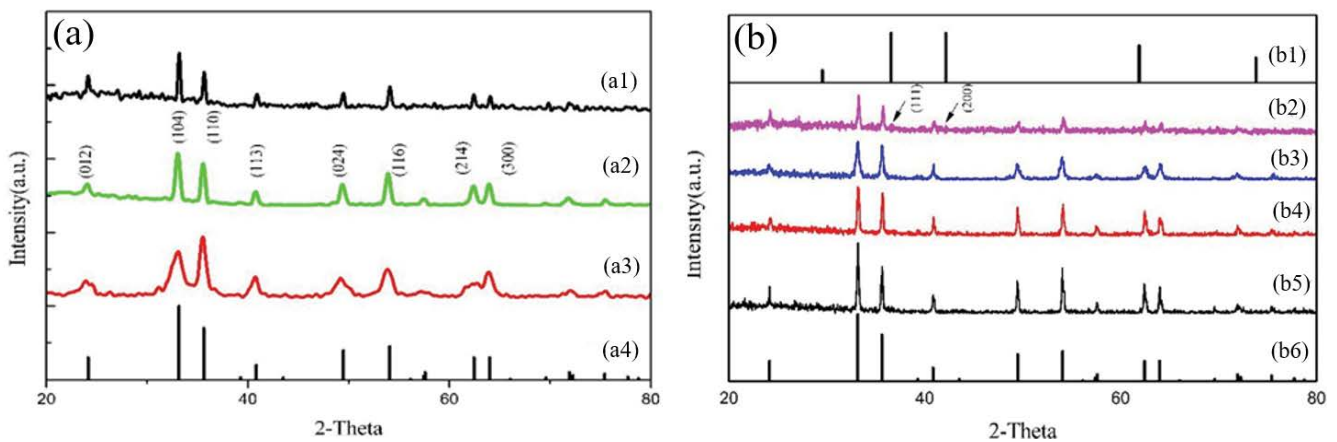


Fig. 3. X-ray diffraction patterns of $\alpha\text{-Fe}_2\text{O}_3$ with different prepare methods (a1) C1, (a2) C2, (a3) C3, (a4) bare $\alpha\text{-Fe}_2\text{O}_3$ and X-ray diffraction patterns of $\text{Cu}_2\text{O}/\alpha\text{-Fe}_2\text{O}_3$ with different Cu_2O doping mass ratio (b1) bare Cu_2O , (b2) 20% Cu_2O , (b3) 15% Cu_2O , (b4) 10% Cu_2O , (b5) 5% Cu_2O , and (b6) bare $\alpha\text{-Fe}_2\text{O}_3$.

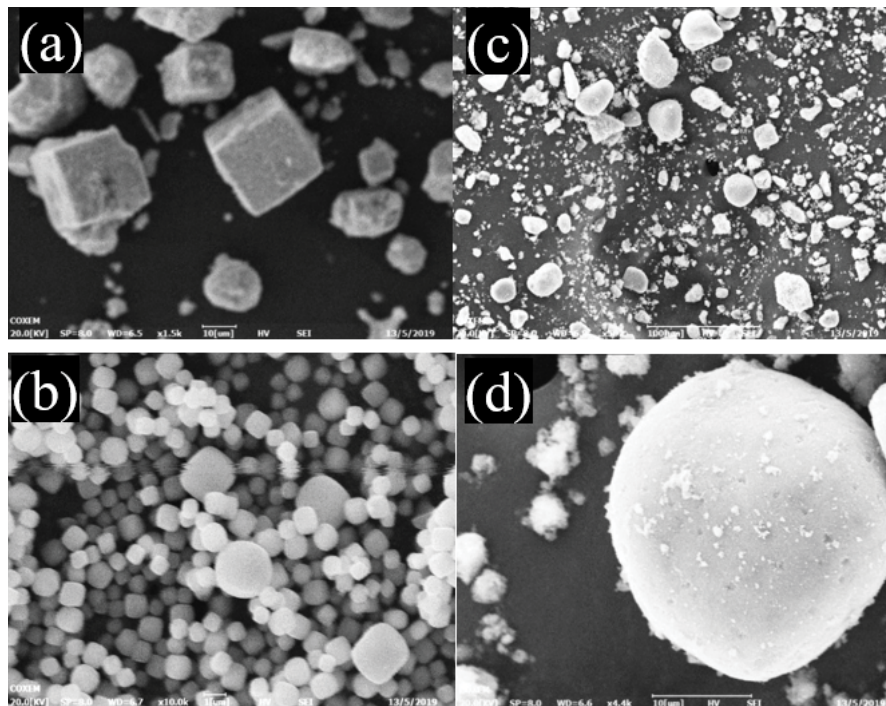


Fig. 4. Scanning electron microscopy graphs of photocatalyst (a) C1, (b) C2, (c) C3, and (d) $\text{Cu}_2\text{O}/\alpha\text{-Fe}_2\text{O}_3$ composite.

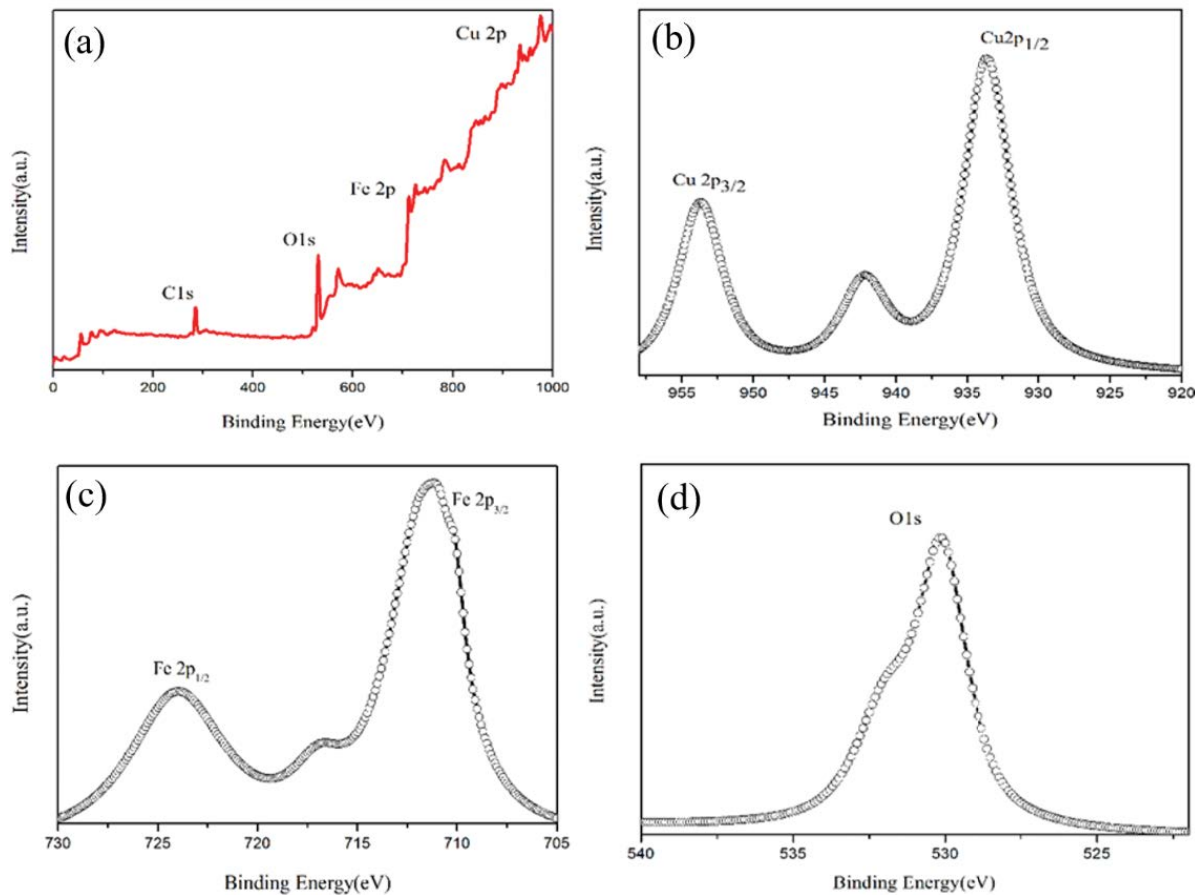


Fig. 5. X-ray photoelectron spectroscopy spectra of $\text{Cu}_2\text{O}/\alpha\text{-Fe}_2\text{O}_3$ samples: (a) survey scan, (b) Cu2p, (c) Fe2p, and (d) O1s.

the C1s signal of pollutant carbon with a binding energy of 284.6 eV. The main peaks observed at 284.6, 530.1, 933.4, and 711.2 eV can be assigned to C1s, O1s, $\text{Cu}2p_{3/2}$ and $\text{Fe}2p_{3/2}$, respectively. The carbon 1s peak is produced by the carbon band used in the XPS instrument, and Fig. 5d shows the O1s peak at 530.1 eV is produced by the lattice oxygen of Cu_2O [29]. Fig. 5b shows the characteristic peaks of Cu_2O at the bound energies of 933.4 eV and 953.6 eV, respectively. Some shifts have been made to the contrast $\text{Cu}2p_{3/2}$ and $\text{Cu}2p_{1/2}$. This may be due to the low doping amount of Cu_2O and the formation of a small amount of Cu^{2+} . A broad satellite peak was also observed around 940–945 eV which indicating the presence of a CuO phase [30]. However, the peak of the Cu_2O phase is much stronger than CuO, so the copper oxide mainly exists in the Cu^+ phase of the photocatalyst. It has been reported that the existence of the CuO phase may be caused by the surface oxidation of Cu_2O particles in the surrounding atmosphere. Fig. 5c shows the peaks of 724.0 eV and 711.2 eV correspond to $\text{Fe}2p_{1/2}$ and $\text{Fe}2p_{3/2}$, respectively.

2.5.4. Congo red ultraviolet absorption spectrum

From Fig. 6a, 30 mg L^{-1} Congo red solution was studied by wavelength scanning from 200 to 800 nm, and the UV-visible absorption spectrum was measured after zero

calibration. It was found that Congo red strong absorption peaks at 328 and 497 nm, respectively. Fig. 6b shows the UV-Vis absorption spectrum of Congo red has a maximum absorption peak at 497 nm. Fig. 6c shows that at 497 nm the concentration of Congo red solution has a good linear relationship with its absorbance, and its concentration can be obtained by the absorbance of Congo red at 497 nm. Subsequent experiments were conducted at this wavelength.

3. Results and discussion

3.1. Catalyst synthesis method

The photocatalytic properties of three kinds of iron oxide C1, C2 and C3 synthesized by the hydrothermal method were measured, and under high-pressure mercury lamp irradiation, reaction temperature of 25°C, pH = 7.0, catalyst dosage of 10 mg and of Congo red initial concentration of 30 mg L^{-1} , the Congo red degradation rate of C1, C2 and C3 for 60 min are shown in Fig. 7a.

Fig. 7a shows that the preparation of the C1 nanometer iron oxide by the first method has only a strong photocatalytic effect on the beginning, and the degradation efficiency is lower at the later stage, the degradation rate can reach only 11.31%. The C2 photocatalyst was prepared by the second method has a strong degradation effect and

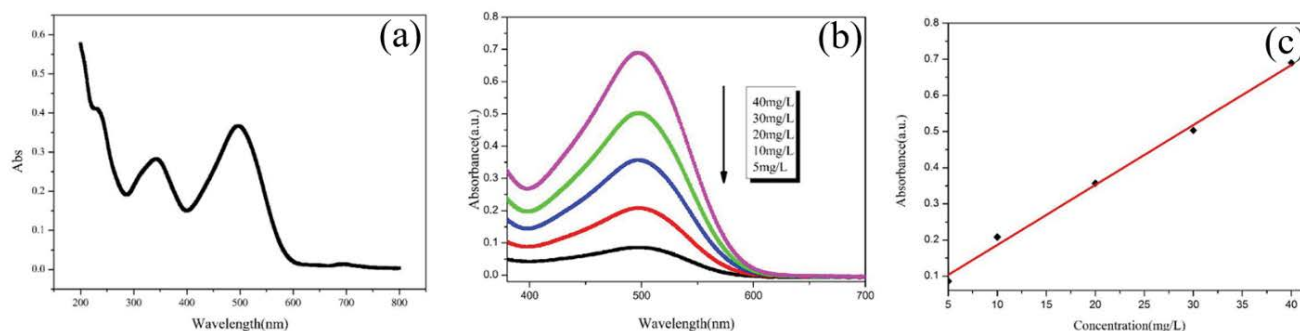


Fig. 6. Congo red ultraviolet absorption spectrum (a), Congo red concentration and absorption wavelength change (b) and linear relationship between Congo red concentration and absorbance (c).

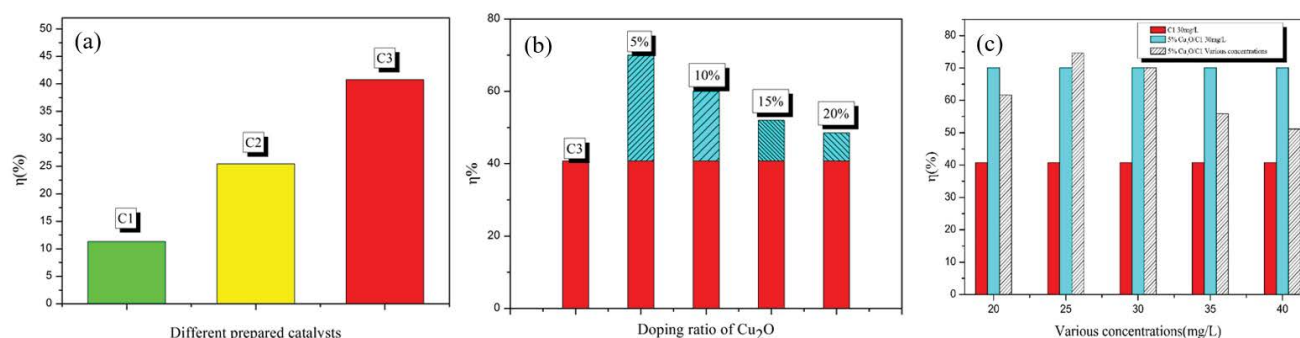


Fig. 7. Degradation rate of Congo red by different catalyst systems (a), degradation rate of Congo red in different doping ratio of Cu_2O (b) and effect of different Congo red concentrations on degradation rate (c).

the degradation rate can up to 25.45%. The C3 photocatalyst prepared by the third method has a very high degradation rate at a later stage and has a strong photocatalytic activity, the Congo red degradation rate can obtain 40.75%. Combined with SEM photos analysis, the surface structure of nano-iron oxide prepared has few defects, and the incompleteness is beneficial to improve its photocatalytic performance. It is possible that the surface defects of photocatalytic materials are beneficial to increase the contact area with Congo red, which is beneficial to light irradiation and absorption. Photogenerated electron-hole pairs improve the photocatalytic efficiency of nano-iron oxide. Therefore, the iron oxide required for the preparation of the subsequent composite material (C3) is prepared by the third method.

3.2. Raw material ratio

In this experiment, composite materials with different $\text{Cu}_2\text{O}/\alpha\text{-Fe}_2\text{O}_3$ mass ratios were prepared. Under the temperature of 25°C, pH = 7.0, catalyst dosage of 10 mg and initial Congo red concentration of 30 mg L^{-1} , Congo red was degraded by mercury lamp illumination for 60 min under the different Cu_2O mass ratio composites. The photocatalytic efficiency of $\text{Cu}_2\text{O}/\alpha\text{-Fe}_2\text{O}_3$ composite catalysts with different mass ratios of cuprous oxide is shown in Fig. 7b.

Fig. 7b shows that the Cu_2O mass ratio is 0%, 5%, 10%, 15% and 20% composite materials obtained by the composite process have stronger photocatalytic properties, the reaction degradation rate can up to 40.75%, 70.06%, 59.87%, 52.01% and 48.48%, respectively. The probable reason may

be *p*-type semiconductor Cu_2O and *n*-type semiconductor $\alpha\text{-Fe}_2\text{O}_3$ can form the *p-n* heterojunction on the interface, thus establishing an internal electric field from $\alpha\text{-Fe}_2\text{O}_3$ to Cu_2O at the interface. Under visible light illumination, electron-hole pairs are generated on $\alpha\text{-Fe}_2\text{O}_3$ and Cu_2O . The electrons on the conduction band of $\alpha\text{-Fe}_2\text{O}_3$ are transferred to the conduction band of Cu_2O , and react with oxygen to generate hydroxyl radicals. The holes on $\alpha\text{-Fe}_2\text{O}_3$ and Cu_2O interact with water to generate hydroxyl radicals. These radical groups undergo redox reactions with organic molecules, thereby degrading Congo red molecules [31]. Even the photocatalytic performance of 0% pure iron oxide C3 has been significantly improved. It may be possible to change the surface structure of the product C3 nanometer iron oxide through the composite process operation and improve its photocatalytic performance. When the Cu_2O mass ratio is 5%, the photocatalytic performance of the $\text{Cu}_2\text{O}/\alpha\text{-Fe}_2\text{O}_3$ composite catalyst is the highest, and the degradation rate of Congo red can up to 70.06%. With the increase of Cu_2O content, the photocatalytic performance of the composite material is reduced, from the Cu_2O mass ratio 10% to 20%, the degradation rate can reach 59.87% to 48.48%. Therefore, the optimized content of cuprous oxide in the composite photocatalyst is 5% in subsequent experiments.

3.3. Effect of initial concentration

Under the conditions of temperature (25°C), pH = 7.0, catalyst dosage of 10 mg and composite ratio (Cu_2O mass ratio 5%), high-pressure mercury lamp illumination reaction

60 min, the effects of different initial Congo red concentration of 20, 25, 30, 35, and 40 mg L⁻¹ on the degradation rate of Congo red were investigated. The results are shown in Fig. 7c.

As can be seen from Fig. 7c, when Congo red concentration is 25 mg L⁻¹, the maximum degradation rate was obtained. When Congo red solution concentration is 20 mg L⁻¹, the photocatalytic degradation rate of the Cu₂O/ α -Fe₂O₃ composite photocatalyst is 61.66%, and when Congo red solution concentration is 25 mg L⁻¹, the degradation rate rose to 74.63%. This is because during the rise of Congo red concentration, the contact probability of Cu₂O/ α -Fe₂O₃ composites with Congo red molecules is increasing, and the activity of photocatalytic degradation is also increased.

When the Congo red concentration was continued to increase to 30 mg L⁻¹, the degradation rate decreased to 70.06%. Then increase the solubility of Congo red solution, the degradation rate of the Cu₂O/ α -Fe₂O₃ composites in the degradation of 35 and 40 mg L⁻¹ solution decreased to 55.90% and 51.16%, respectively. The reason is that, as the initial concentration of the Congo red solution increases, photocatalyst can generate electron and hole pairs, during the photocatalytic reaction electron-hole pairs are saturated. On the other hand, initial Congo red concentration increases, it is more difficult to produce a photocatalytic reaction when the solution is irradiated by high-pressure light source. For the above reasons, the amount of hydroxyl radicals generated by the Cu₂O/ α -Fe₂O₃ composite photocatalyst under the high-pressure mercury lamp is limited. As the concentration of the Congo red solution increases, the number of reactant molecules increases, the color of the Congo red gradually darkens, and the absorption of visible light by the photocatalyst is correspondingly weakened. So, the optimal Congo red initial concentration is 25 mg L⁻¹, the photocatalytic efficiency of the composite material can reach 74.63%.

3.4. Amount of catalyst

In this experiment, under the conditions of room temperature (25°C), pH = 7.0, initial Congo Red concentration of 25 mg L⁻¹ and 5% Cu₂O mass ratio of composite catalyst, under the high-pressure mercury lamp irradiation, reaction 60 min. The different catalysts quality of 5, 8, 10, 12 and 15 mg were added to the photocatalytic reaction system were studied. The degradation rate of Congo red is shown in Fig. 8a.

When the added amount of photocatalyst is 5 mg, the degradation efficiency of Cu₂O/ α -Fe₂O₃ composite is only 35.56%. As the amount of catalyst increases from 8 mg, 10 mg to 12 mg, the degradation rate of composite increases gradually to reach 72.75%, 74.63% and 89.80%, respectively. This is because the more photocatalyst added, the more contact area of Cu₂O/ α -Fe₂O₃ composite with Congo red and the increased their reaction probability, thereby increases the photocatalytic degradation activity. When a larger amount of composite material was added, the degradation efficiency was reduced to 85.34%. Although there is sufficient contact between the composite photocatalyst and the Congo red molecules, the excess composite photocatalyst will stay in the dye wastewater solution and make the solution turbid. Therefore, the light transmittance of the solution becomes poor, which is not conducive to the photocatalytic reaction, thereby reducing the Congo red degradation rate.

3.5. Effect of temperature

Under the conditions of pH 7.0, catalyst dosage of 12 mg, initial Congo red concentration of 25 mg L⁻¹ and 5% Cu₂O mass ratio composite catalyst, the effect of different temperatures of 25°C, 30°C, 35°C, 40°C and 45°C on the photodegradation rates were measured. The results are shown in Fig. 8b.

Fig. 8b shows that the temperature from 25°C to 30°C, the Congo red degradation rate can both up to 90%. When the temperature is between 30°C and 45°C, the degradation rates decreases slowly with the increase of temperature, and the degradation rate can reach 80%. The reason is that, the temperature increases, the activated molecules move vigorously, and the reaction rate increases. However, if the temperature is too high, it may be accompanied by side reactions or damage to the catalyst structure. Therefore, the optimal reaction temperature of the composite photocatalyst is 25°C, and degradation performance is good in this temperature range.

3.6. Kinetics analysis

According to the Langmuir–Hinshelwood dynamic equation:

$$r = -\frac{dc}{dt} = \frac{kKc_i}{1 + Kc_i} \quad (2)$$

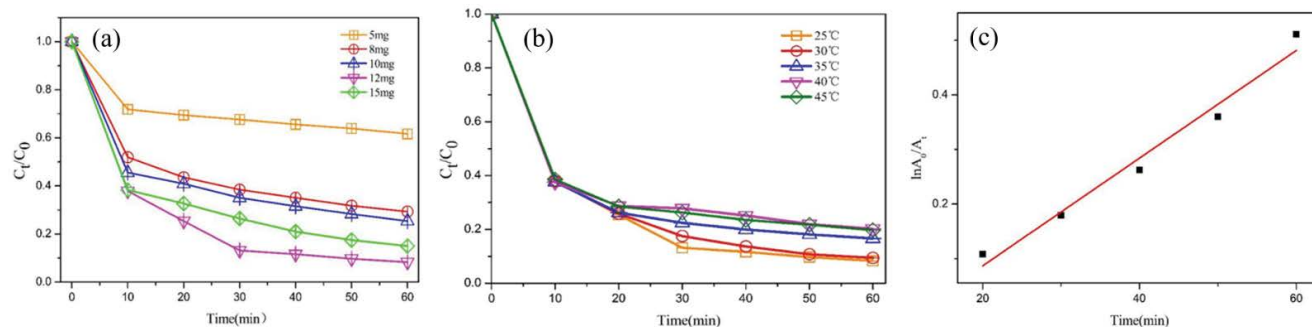


Fig. 8. Effect of different catalyst dosage on Congo red degradation rate (a) and Congo red degradation rate at different temperatures (b) and dynamic analyses linear relationship diagram (c).

where K is the adsorption equilibrium constant, L mg^{-1} ; k is the reaction rate constant, $\text{mg L}^{-1} \text{min}^{-1}$; r is the reaction rate at a certain time; c_t is the reaction concentration at t time, mg L^{-1} .

In this heterogeneous catalytic reaction, the slope of the curve is the largest when the initial concentration is low, the degradation rate of Congo red is the fastest, this suggests that the control step is the surface reaction step of the composite catalyst and the influence of the intermediate product on the reaction is negligible. That is, much less than 1. So the above formula can be converted into:

$$r = -\frac{dc}{dt} = kKc_i = k'c_i \quad (3)$$

Integral:

$$\ln \frac{c_0}{c_t} = k't \quad (4)$$

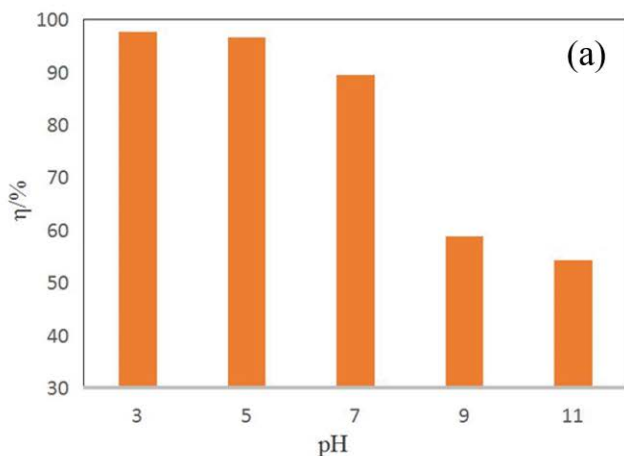
where k' is the first-order kinetic constant, min^{-1} , according to the $A = \epsilon bc$:

$$\ln \frac{A_0}{A_t} = \ln \frac{c_0}{c_t} = k't \quad (5)$$

Fig. 8c can be used to determine the relationship between $\ln A_0/A_t$ and time. Fitting equation $y = 0.0099x - 0.1103$, first-order kinetic constant k' is 0.0099 min^{-1} . Therefore, the photocatalytic reaction mechanism of composite materials degrading Congo red at 25°C accords with the quasi-first-order kinetic equation.

3.7. Effect of initial pH

In this experiment, the photocatalytic experiments were carried out under the room temperature of 25°C , catalyst dosage of 12 mg , initial Congo red concentration of 25 mg L^{-1} and 5% Cu_2O mass ratio composite photocatalyst.



The effect of initial pH values of 3.0, 5.0, 7.0, 9.0, and 11.0 were studied. The results of Congo red degradation rate data as shown in Fig. 9a.

It can be seen from Fig. 9a, the photocatalytic degradation performance of the composite material under acidic conditions is better than the alkali conditions, it can be reached more than 90%. Therefore, the Congo red degradation rate under acidic conditions was studied, and the results are shown in Fig. 9b.

From Fig. 9b we can see that the degradation rate of pH below 6.0 is hardly changed. The degradation rate of Congo red by composites is over 95.57% of pH 6.0 is higher than that of 89.80% of pH 7.0. This is because under acidic conditions, superoxide radicals react with H^+ to form water radicals and water radicals in the solution to form hydrogen peroxide and oxygen. Hydrogen peroxide has strong oxidizing properties and more hydrogen peroxide in the solution. Congo red can be better degraded. Since the prepared composite material is a metal oxide, it may react to the composite material in the case of peracid, and the composite material are deactivated. Therefore, the optimal pH condition for subsequent experiments is 6.0.

3.8. Chemical oxygen demand and total organic carbon removal

To clarify the reaction mechanism of photocatalytic degradation of Congo red, the chemical oxygen demand (COD) and total organic carbon (TOC) removal rates under optimized degradation conditions were analyzed. The curves of COD and TOC removal rates with time are shown in Fig. 10. COD was measured on a JH-12 COD analysis apparatus and COD removal percentage were calculated with the following equation:

$$\text{COD removal\%} = \frac{\text{COD}_0 - \text{COD}_t}{\text{COD}_0} \times 100 \quad (6)$$

where COD_0 is the COD value of the initial Congo red solution (mg L^{-1}), and COD_t is the COD value of the Congo red solution after t min (mg L^{-1}).

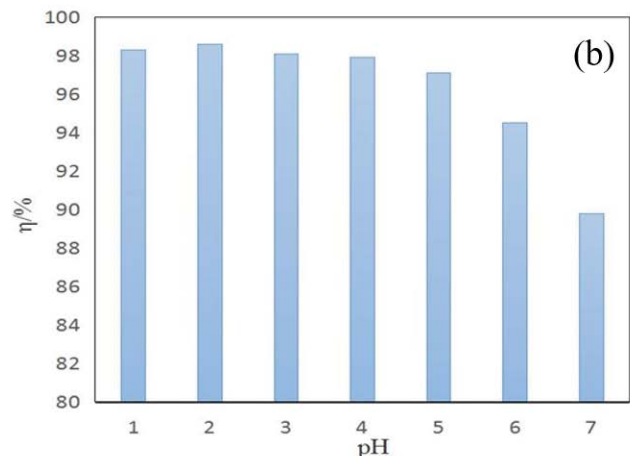


Fig. 9. Photocatalytic performance of $\text{Cu}_2\text{O}/\alpha\text{-Fe}_2\text{O}_3$ composites at different pH (a) and degradation rate of Congo red under acidic conditions (b).

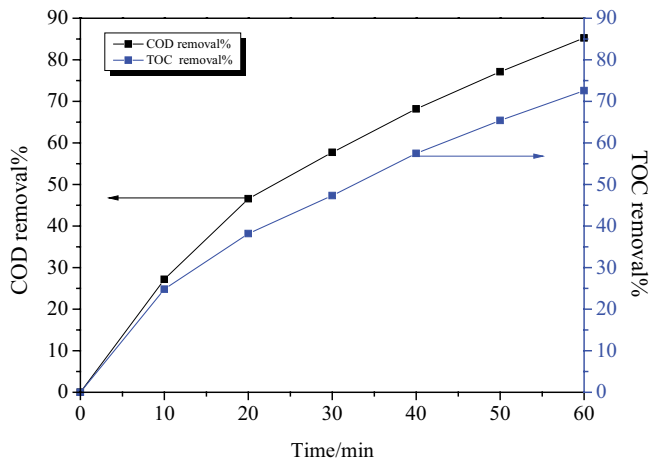


Fig. 10. Chemical oxygen demand and total organic carbon removal under the optimal degradation rate.

TOC Analyzer was used to measure TOC concentration according to National Environmental Protection Agency (1991), for which the standard is GB (HJ501-2009). All samples were diluted 10 times before analysis. The TOC removal percentage of Congo red was calculated by the following equation:

$$\text{TOC removal\%} = \frac{\text{TOC}_0 - \text{TOC}_t}{\text{TOC}_0} \times 100 \quad (7)$$

where TOC_0 is the value of the initial Congo red solution (mg L^{-1}), and TOC_t is the TOC value of the Congo red solution after t min (mg L^{-1}).

Fig. 10 shows that the results of COD and TOC removal both show an increasing trend during the photocatalytic degradation of Congo red by the $\text{Cu}_2\text{O}/\alpha\text{-Fe}_2\text{O}_3$ composite photocatalyst. After reaction 60 min, the removal rates of COD and TOC can reach 85.36% and 72.57%, respectively. We can preliminarily judge that most of Congo red dye has been degraded and a part of it has been mineralized to carbon dioxide and water.

3.9. Possible mechanism for the photocatalytic actions

The mechanism of enhancing photocatalytic performance of $\text{Cu}_2\text{O}/\alpha\text{-Fe}_2\text{O}_3$ composite materials was elucidated, it is necessary to study the band structure of each component of $\text{Cu}_2\text{O}/\alpha\text{-Fe}_2\text{O}_3$ composite material. The schematic diagram of a possible photocatalytic mechanism is shown in Fig. 11.

The possible reaction equations are as follows:

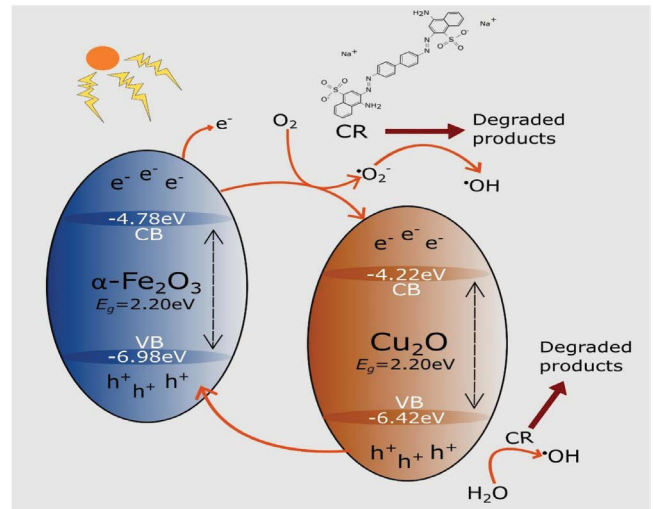
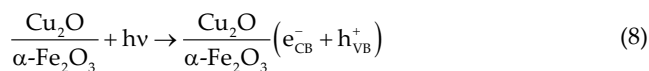
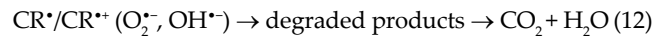


Fig. 11. Schematic diagram of a possible photocatalytic mechanism of $\text{Cu}_2\text{O}/\alpha\text{-Fe}_2\text{O}_3$.



From Fig. 11, the conduction band (CB) potential of $\alpha\text{-Fe}_2\text{O}_3$ is -4.78 eV, more negative than that of Cu_2O (-4.22 eV). Therefore, electrons diffuse from CB of $\alpha\text{-Fe}_2\text{O}_3$ to Cu_2O easily. At the same time, since the valence band (VB) potential of Cu_2O is more positive than the VB potential of the $\alpha\text{-Fe}_2\text{O}_3$, the holes are more easily transferred from the VB of Cu_2O to $\alpha\text{-Fe}_2\text{O}_3$, forming a similar closed-loop reaction system [32]. Thereby, photo-generated electrons and holes are effectively separated at the heterojunction. Photogenerated holes occupy the main photon energy, react with hydroxide or water molecules attached to the catalyst surface to generate active hydroxyl radicals, and photogenerated electrons transfer to form superoxide radicals with the oxygen in the adsorption solution. Hydroxyl radicals and superoxide radicals are both strong oxidative reactive groups that can oxidize Congo red dye molecules.

4. Conclusions

In this experiment, $\alpha\text{-Fe}_2\text{O}_3$ was prepared by hydrothermal method and $\text{Cu}_2\text{O}/\alpha\text{-Fe}_2\text{O}_3$ composites were synthesized by precipitation method. Congo red was used as the simulated dye wastewater. The photocatalytic activity of $\text{Cu}_2\text{O}/\alpha\text{-Fe}_2\text{O}_3$ prepared is obviously improved compared with single $\alpha\text{-Fe}_2\text{O}_3$. Under the high-pressure mercury lamp illumination, the pH value is 6.0, the reaction temperature is 25°C and the amount of $\text{Cu}_2\text{O}/\alpha\text{-Fe}_2\text{O}_3$ catalyst is 12 mg, photocatalytic degradation 100 mL 30 mg L^{-1} Congo red for 60 min, the degradation rate can reach 95.57%. The removal rates of COD and TOC can up to 85.36% and 72.57%, respectively. Under the optimized conditions, the degradation of Congo red matches the quasi-first order reaction. The introduction of Cu_2O plays the role of bridge-chain, which can effectively inhibit the recombination of photo-generated electron and hole pairs, thereby improving the composite photocatalyst performance.

Acknowledgments

We acknowledge the financial sponsorship by the Fundamental Research Funds for the Central Universities (2572015CB23) and the China Postdoctoral Science Foundation-funded project (2014 M561312). We also gratefully acknowledge the support of the Natural Science Foundation of China (51602046), the Postdoctoral Foundation of Heilongjiang Province of China (LBH-Z14014) and the Scientific Research Project of Harbin Science and Technology Bureau (2015RQXJ063) and the China scholarship council program (2019066005013).

References

- [1] A. Fujishima, X.T. Zhang, D.A. Tryk, TiO₂ photocatalysis and related surface phenomena, *Surf. Sci. Rep.*, 63 (2008) 515–582.
- [2] R. Saravanan, E. Sacari, F. Gracia, M.M. Khan, E. Mosquera, V.K. Gupta, Conducting PANI stimulated ZnO system for visible light photocatalytic degradation of coloured dyes, *J. Mol. Liq.*, 221 (2016) 1029–1033.
- [3] W.J. Ren, Z.H. Ai, F.L. Jia, L.Z. Zhang, X.X. Fan, Z.G. Zou, Low temperature preparation and visible light photocatalytic activity of mesoporous carbon-doped crystalline TiO₂, *Appl. Catal., B*, 69 (2007) 138–144.
- [4] H. Seema, K.C. Kemp, V. Chandra, K.S. Kim, Graphene–SnO₂ composites for highly efficient photocatalytic degradation of Methylene blue under sunlight, *Nanotechnology*, 23 (2012) 355705, doi: 10.1088/0957-4484/23/35/355705.
- [5] Q.H. Liu, Q. Cao, H. Bi, C.Y. Liang, K.P. Yuan, W. She, Y.J. Yang, R.C. Che, CoNi@SiO₂@TiO₂ and CoNi@Air@TiO₂ microspheres with strong wideband microwave absorption, *Adv. Mater.*, 28 (2016) 486–490.
- [6] J.X. Low, B. Cheng, J.G. Yu, Surface modification and enhanced photocatalytic CO₂ reduction performance of TiO₂: a review, *Appl. Surf. Sci.*, 392 (2017) 658–686.
- [7] K. Li, S.M. Gao, Q.Y. Wang, H. Xu, Z.Y. Wang, B.B. Huang, Y. Dai, J. Lu, *In-situ*-reduced synthesis of Ti³⁺ self-doped TiO₂/g-C₃N₄ heterojunctions with high photocatalytic performance under LED light irradiation, *ACS Appl. Mater. Interfaces*, 7 (2015) 9023–9030.
- [8] J.L. Zhang, L.S. Zhang, X.F. Shen, P.F. Xu, J.S. Liu, Synthesis of BiOBr/WO₃ *p-n* heterojunctions with enhanced visible light photocatalytic activity, *Cryst. Eng. Commun.*, 18 (2016) 3856–3865.
- [9] S.G. Babu, R. Vinoth, P.S. Narayana, D. Bahnemann, B. Neppolian, Reduced graphene oxide wrapped Cu₂O supported on C₃N₄: an efficient visible light responsive semiconductor photocatalyst, *APL Mater.*, 3 (2015) 104415, <https://doi.org/10.1063/1.4928286>.
- [10] S.G. Kumar, K.S.R. Koteswara Rao, Comparison of modification strategies towards enhanced charge carrier separation and photocatalytic degradation activity of metal oxide semiconductors (TiO₂, WO₃ and ZnO), *Appl. Surf. Sci.*, 391 (2017) 124–148.
- [11] T.S. Natarajan, K. Natarajan, H.C. Bajaj, R.J. Tayade, Energy efficient UV-LED source and TiO₂ nanotube array-based reactor for photocatalytic application, *Ind. Eng. Chem. Res.*, 50 (2011) 7753–7762.
- [12] H.L. Wang, L.S. Zhang, Z.G. Chen, J.Q. Hu, S.J. Li, Z.H. Wang, J.S. Liu, X.C. Wang, Semiconductor heterojunction photocatalysts: design, construction, and photocatalytic performances, *Chem. Soc. Rev.*, 43 (2014) 5234–5244.
- [13] W.D. Chemelewski, O. Mabayoje, D. Tang, A.J.E. Rettie, C. Buddie Mullins, Bandgap engineering of Fe₂O₃ with Cr - application to photoelectrochemical oxidation, *Phys. Chem. Chem. Phys.*, 18 (2016) 1644–1648.
- [14] M.B. Sahana, C. Sudakar, G. Setzler, A. Dixit, J.S. Thakur, G. Lawes, R. Naik, V.M. Naik, P.P. Vaishnava, Bandgap engineering by tuning particle size and crystallinity of SnO₂-Fe₂O₃ nanocrystalline composite thin films, *Appl. Phys. Lett.*, 93 (2008) 231909, <https://doi.org/10.1063/1.3042163>.
- [15] A.D. Bokare, W.Y. Choi, Review of iron-free Fenton-like systems for activating H₂O₂ in advanced oxidation processes, *J. Hazard. Mater.*, 275 (2014) 121–135.
- [16] M. Mishra, D.-M. Chun, α -Fe₂O₃ as a photocatalytic material: a review, *Appl. Catal., A*, 498 (2015) 126–141.
- [17] X.J. She, J.J. Wu, H. Xu, J. Zhong, Y. Wang, Y.H. Song, K.Q. Nie, Y. Liu, Y.C. Yang, M.-T.F. Rodrigues, R. Vajtai, J. Lou, D.L. Du, H.M. Li, P.M. Ajayan, High efficiency photocatalytic water splitting using 2D α -Fe₂O₃/g-C₃N₄ Z-scheme catalysts, *Adv. Energy Mater.*, 7 (2017) 1700025, <https://doi.org/10.1002/aenm.201700025>.
- [18] J. Liu, S.L. Yang, W. Wu, Q.Y. Tian, S.Y. Cui, Z.G. Dai, F. Ren, X.H. Xiao, C.Z. Jiang, 3D flowerlike α -Fe₂O₃@TiO₂ core-shell nanostructures: general synthesis and enhanced photocatalytic performance, *ACS Sustainable Chem. Eng.*, 3 (2015) 2975–2984.
- [19] Y.Y. Liu, W. Jin, Y.P. Zhao, G.S. Zhang, W. Zhang, Enhanced catalytic degradation of Methylene blue by α -Fe₂O₃/graphene oxide via heterogeneous photo-Fenton reactions, *Appl. Catal., B*, 206 (2017) 642–652.
- [20] J. Zhao, Q.F. Lu, M.Z. Wei, C.Q. Wang, Synthesis of one-dimensional α -Fe₂O₃/Bi₂MoO₆ heterostructures by electrospinning process with enhanced photocatalytic activity, *J. Alloys Compd.*, 646 (2015) 417–424.
- [21] S.C. Siah, Y.S. Lee, Y. Segal, T. Buonassisi, Low contact resistivity of metals on nitrogen-doped cuprous oxide (Cu₂O) thin-films, *J. Appl. Phys.*, 112 (2012) 084508, <https://doi.org/10.1063/1.4758305>.
- [22] Z.K. Zheng, B.B. Huang, Z.Y. Wang, M. Guo, X.Y. Qin, X.Y. Zhang, P. Wang, Y. Dai, Crystal faces of Cu₂O and their stabilities in photocatalytic reactions, *J. Phys. Chem. C*, 113 (2009) 462–470.
- [23] H.Y. Zheng, Q. Li, Y.P. Zhang, L.Z. Qin, H. Lin, M. Nie, Convenient and green soft chemical route to cuprous oxide films and their visible-light photocatalytic properties, *Micro Nano Lett.*, 10 (2015) 554–557.
- [24] M.A. Nguyen, N.M. Bedford, Y. Ren, E.M. Zahran, R.C. Goodin, F.F. Chagani, L.G. Bachas, M.R. Knecht, Direct synthetic control over the size, composition, and photocatalytic activity of octahedral copper oxide materials: correlation between surface structure and catalytic functionality, *ACS Appl. Mater. Interfaces*, 7 (2015) 13238–13250.
- [25] S.T. Ren, G.L. Zhao, Y.Y. Wang, B.Y. Wang, Q. Wang, Enhanced photocatalytic performance of sandwiched ZnO@Ag@Cu₂O nanorod films: the distinct role of Ag NPs in the visible light and UV region, *Nanotechnology*, 26 (2015) 125403, doi: 10.1088/0957-4484/26/12/125403.
- [26] J.-C. Wang, L. Zhang, W.-X. Fang, J. Ren, Y.-Y. Li, H.-C. Yao, J.-S. Wang, Z.-J. Li, Enhanced photoreduction CO₂ activity over direct Z-scheme α -Fe₂O₃/Cu₂O heterostructures under visible light irradiation, *ACS Appl. Mater. Interfaces*, 7 (2015) 8631–8639.
- [27] S.K. Lakhera, A. Watts, H.Y. Hafeez, B. Neppolian, Interparticle double charge transfer mechanism of heterojunction α -Fe₂O₃/Cu₂O mixed oxide catalysts and its visible light photocatalytic activity, *Catal. Today*, 300 (2018) 58–70.
- [28] H.L. Xu, W.Z. Wang, Template synthesis of multishelled Cu₂O hollow spheres with a single-crystalline shell wall, *Angew. Chem. Int. Ed.*, 46 (2007) 1489–1492.
- [29] H. Meng, W. Yang, K. Ding, L. Feng, Y.F. Guan, Cu₂O nanorods modified by reduced graphene oxide for NH₃ sensing at room temperature, *J. Mater. Chem. A*, 3 (2015) 1174–1181.
- [30] S.W. Lee, Y.S. Lee, J.Y. Heo, S.C. Siah, D. Chua, R.E. Brandt, S.B. Kim, J.P. Mailoa, T. Buonassisi, R.G. Gordon, Improved Cu₂O-based solar cells using atomic layer deposition to control the Cu oxidation state at the *p-n* junction, *Adv. Energy Mater.*, 4 (2014) 1301916, <https://doi.org/10.1002/aenm.201301916>.
- [31] M. Yin, C.-K. Wu, Y.B. Lou, C. Burda, J.T. Koberstein, Y.M. Zhu, S. O'Brien, Copper oxide nanocrystals, *J. Am. Chem. Soc.*, 127 (2005) 9506–9511.
- [32] Y.K. Kwon, A.S. Soon, H.S. Han, H.J. Lee, Shape effects of cuprous oxide particles on stability in water and photocatalytic water splitting, *J. Mater. Chem. A*, 3 (2015) 156–162.